

**RESEARCH LETTER**

10.1002/2016GL070776

**Key Points:**

- Shallow convection fields provided by LES coupled with a radar simulator were studied
- A new objective method of estimating domain-averaged cloud fraction profiles using scanning cloud radar was proposed
- Cloud fraction profiles from a single zenith cloud radar are subject to large uncertainties

**Correspondence to:**

M. Oue,  
mariko.oue@stonybrook.edu

**Citation:**

Oue, M., P. Kollias, K. W. North, A. Tatarevic, S. Endo, A. M. Vogelmann, and W. I. Gustafson Jr. (2016), Estimation of cloud fraction profile in shallow convection using a scanning cloud radar, *Geophys. Res. Lett.*, *43*, 10,998–11,006, doi:10.1002/2016GL070776.

Received 24 JUN 2016

Accepted 21 SEP 2016

Accepted article online 23 SEP 2016

Published online 18 OCT 2016

## Estimation of cloud fraction profile in shallow convection using a scanning cloud radar

Mariko Oue<sup>1</sup>, Pavlos Kollias<sup>1,2</sup>, Kirk W. North<sup>3</sup>, Aleksandra Tatarevic<sup>3</sup>, Satoshi Endo<sup>2</sup>, Andrew M. Vogelmann<sup>2</sup>, and William I. Gustafson Jr.<sup>4</sup>

<sup>1</sup>School of Marine and Atmospheric Sciences, Stony Brook University, Stony Brook, New York, USA, <sup>2</sup>Environmental and Climate Sciences Department, Brookhaven National Laboratory, Upton, New York, USA, <sup>3</sup>Department of Atmospheric and Oceanic Sciences, McGill University, Montreal, Quebec, Canada, <sup>4</sup>Atmospheric Sciences and Global Change Division, Pacific Northwest National Laboratory, Richland, Washington, USA

---

**Abstract** Large spatial heterogeneities in shallow convection result in uncertainties in estimations of domain-averaged cloud fraction profiles (CFP). This issue is addressed by using large eddy simulations of shallow convection over land coupled with a radar simulator. Results indicate that zenith profiling observations are inadequate to provide reliable CFP estimates. Use of scanning cloud radar (SCR), performing a sequence of cross-wind horizon-to-horizon scans, is not straightforward due to the strong dependence of radar sensitivity to target distance. An objective method for estimating domain-averaged CFP is proposed that uses observed statistics of SCR hydrometeor detection with height to estimate optimum sampling regions. This method shows good agreement with the model CFP. Results indicate that CFP estimates require more than 35 min of SCR scans to converge on the model domain average. The proposed technique is expected to improve our ability to compare model output with cloud radar observations in shallow cumulus cloud conditions.

---

### 1. Introduction

Shallow convection plays a critical role in the heat and moisture transfer between the boundary layer and free atmosphere [e.g., *Browning et al.*, 1993; *Zhang and Klein*, 2013]. Despite their low cloud fraction, shallow cumuli also have an important role in modulating shortwave radiative forcing [*Berg et al.*, 2011]. However, with an average spatial scale of 0.5–1.5 km [e.g., *Lamer and Kollias*, 2015], shallow cumuli are not resolved in weather forecast and climate models, which rely on parameterizations of the subgrid-scale properties to capture the impact of these clouds on the grid-scale meteorological state. The cloud fraction profile (CFP) is a key property of interest because the fractional cloudiness of a gridbox affects the radiative transfer [e.g., *Albrecht*, 1981; *Larson et al.*, 2001] and the CFP affects the vertical cumulus mass flux [e.g., *de Roode and Bretherton*, 2003; *van Stratum et al.*, 2014].

Large eddy simulation (LES) of shallow cumuli has been used in the past to study cloud field properties and their interaction with the environment [e.g., *Siebesma and Holtslag*, 1996; *Siebesma et al.*, 2003]. The simulated cloud structures and properties are typically evaluated using observations. At the U.S. Department of Energy Atmospheric Radiation Measurement (ARM) Climate Research Facility's Southern Great Plains (SGP) site, several long-term studies of shallow cumuli have been conducted by using aircraft and ground-based observations [*Berg and Kassianov*, 2008; *Vogelmann et al.*, 2012; *Chandra et al.*, 2013; *Zhang and Klein*, 2013; *Lamer and Kollias*, 2015]. Zenith profiling cloud radar and lidar measurements traditionally have been used to provide CFP estimates [e.g., *Hogan et al.*, 2001; *Kollias et al.*, 2009; *Rémillard et al.*, 2012]. CFP estimates from these measurements have been effective for evaluating LES and understanding the climatological properties of shallow cumuli.

In an effort to go beyond the idealized case studies, the modeling community has recently begun using semicontinuously operating LES testbeds to provide day-to-day comparisons between high-resolution models and observations. Such testbeds include the Royal Netherlands Meteorological Institute Parameterization Testbed [*Neggens et al.*, 2012] and the LES ARM Symbiotic Simulation and Observation (LASSO) project [*Gustafson and Vogelmann*, 2015; *Gustafson et al.*, 2016]. However, the spatially heterogeneous distribution of these clouds [*Wood and Field*, 2011] raises questions regarding the ability of short-term (1–3 h) zenith profiling observations to provide a sufficient sampling of the cloud

field. Can profiling observations provide statistically robust estimates of key parameters, such as the domain-averaged CFP of shallow cumuli?

The standard instrumentation at the ARM sites includes Scanning ARM Cloud Radars (SACRs) [Kollias *et al.*, 2014a, 2014b]. The SACRs, similar to other scanning cloud radar systems (e.g., MIRA-35S [Myagkov *et al.*, 2016]), conduct observations beyond the vertical column and thus sample a much larger part of the cloudy atmosphere compared to zenith profiling cloud radars such as the Ka-band ARM Zenith Radar (KAZR) [e.g., Lamer *et al.*, 2013; Borque *et al.*, 2014; Ewald *et al.*, 2015]. While the use of scanning radars is the conventional approach for studying weather phenomena, the application of scanning cloud radars (SCRs) to study shallow cumuli is not straightforward. Radar sensitivity decreases with distance from the radar, which results in an increasing minimum reflectivity ( $Z_{\min}$ ) required for detection:

$$Z_{\min}(r) = C + 20 \log_{10}(r). \quad (1)$$

In this equation,  $Z_{\min}$  is expressed in terms of a logarithmic scale (dBZ) of the range of  $r$  in kilometer (distance from the radar) and the constant  $C$  (in dBZ) depends on the radar system characteristics. Better detection sensitivity results from lower values of  $Z_{\min}$ . Reflectivities of at least  $Z_{\min}(r)$  are detectable by a radar within a range of  $r$  in kilometer. The minimum reflectivity value necessary for detection increases with distance from the radar. The typical maximum range of a SCR is 20 km, and thus, following equation (1), the SCR sensitivity drops by 26 dB at 20 km compared to its sensitivity at 1 km. Since shallow cumuli over land typically have low reflectivities, falling below  $Z_{\min}(r)$  [e.g., Lamer and Kollias, 2015], the strong drop in the SCR sensitivity with range creates the illusion of a cloudier atmosphere closer to the radar location. These issues likely have a greater impact when detecting shallow cumuli compared to deeper, mesoscale precipitation systems or stratocumulus cloud decks due to the large spatial heterogeneity and relatively low liquid water content of shallow cumuli [e.g., Warner, 1955; Blyth, 1993].

This study addresses uncertainties of radar-estimated CFPs owing to these issues. In particular, we define a sampling region as a semicircular area above the radar within which all cloudy gridboxes are detected above a range-dependent minimum reflectivity threshold. A key objective of this work is to find the sampling region, or combination of sampling regions, that best reproduces the actual CFP at the radar site, and we propose an objective method for estimating the domain-averaged CFP under shallow cumulus cloud conditions.

## 2. Data

Cloud field distributions are obtained from large eddy simulations of two shallow cumulus cloud cases over the ARM SGP performed with the Advanced Research Weather Research and Forecasting (WRF) Model [Skamarock *et al.*, 2008]. The two cases have different cloud depths: a shallow cloud case on 22 May 2009, during the Routine ARM Aerial Facility Clouds with Low Optical Water Depths Optical Radiative Observations campaign [Vogelmann *et al.*, 2012], and a relatively deep cloud case on 9 June 2015. Figure 1a shows scene reflectance observed by Moderate Resolution Imaging Spectroradiometer (MODIS) Aqua satellite during 9 June 2015. The satellite imagery shows numerous cumulus clouds around the SGP site. It is worth noting that the KAZR at the SGP Central Facility detected only a fraction of these clouds throughout the day. The WRF cloud fields are used as input to the Cloud Resolving Model Radar Simulator (CR-SIM) [Tatarevic and Kollias, 2015; <http://radarscience.weebly.com/radar-simulators.html>] to simulate KAZR and SACR observations. The simulated radar observations are then used to evaluate the performance of the KAZR and SACR in detecting these clouds.

### 2.1. LES Simulations for Shallow Convection Cases

The WRF LES model settings are similar to Endo *et al.* [2015], but the simulation domains are  $28.8 \text{ km} \times 28.8 \text{ km} \times 5.5 \text{ km}$  with 75 m horizontal grid spacing for the 2009 case and  $25.6 \text{ km} \times 25.6 \text{ km} \times 14.7 \text{ km}$  with 100 m horizontal grid spacing for the 2015 case. The vertical grid spacings for the 2009 and 2015 cases are approximately 40 m and 20 m below 5 km altitude, respectively. The model is initialized with a sounding profile launched from the SGP Central Facility at 12:00 UTC for each case, and large-scale forcing and surface fluxes are from ARM's constrained variational analysis forcing data set [Xie *et al.*, 2004]. The Morrison double moment microphysics scheme was used for both cases, which predicts mixing ratios and number densities for liquid cloud, rain, ice cloud, snow, and graupel hydrometeor species [Morrison *et al.*, 2005].

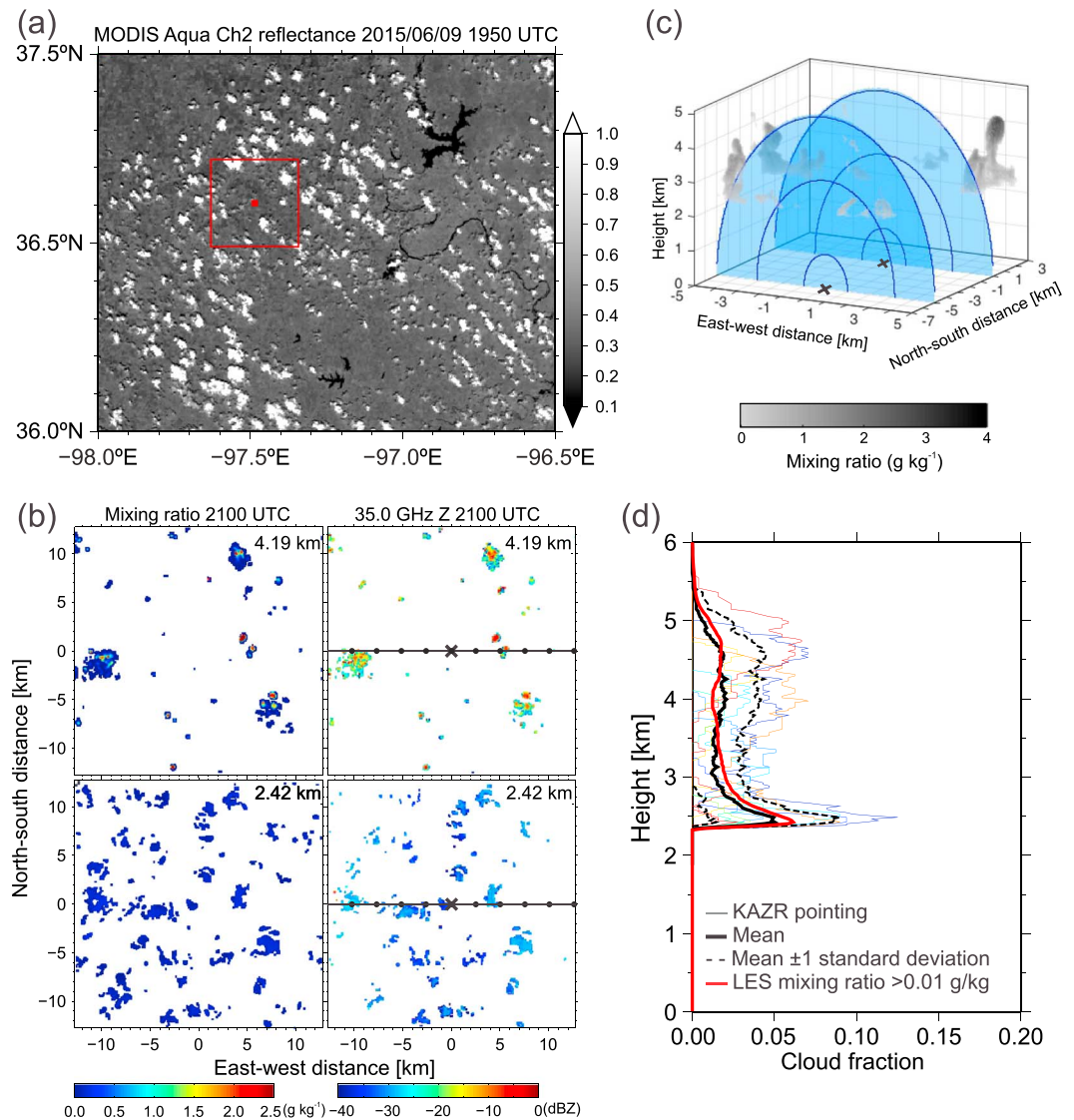


**Figure 1.** (a) MODIS Aqua satellite-observed reflectance on 9 June 2015. The red dot is the location of the SGP Central Facility, and the square region represents the size of LES domain. (b) The horizontal cross sections of hydrometeor mixing ratio from the LES (left column) and Ka-band reflectivity (right column) at 4.19 km (top) and 2.42 km (bottom) above ground level. Xs in Figure 1b represent the center of LES domain and the location of the SACR. Radar sensitivity calculated by equation (1) was applied to the reflectivity plots assuming CWRHI. East-west lines in Figure 1b represent a CWRHI scan. The dots represent the KAZR profiling radar locations that produced cloud fraction profiles in Figure 1d. (c) The conceptual diagram of CWRHI scans. Xs in Figure 1c represent the location of the SACR. Each CWRHI section is represented by the light blue shading together with the blue lines representing radar sensitivity isolines of  $-50$ ,  $-40$ , and  $-36$  dBZ from the vicinity of the radar. Three-dimensional cloud volumes are indicated by gray. (d) Cloud fractions from hydrometeor mixing ratio greater than  $0.01 \text{ g kg}^{-1}$  over the LES domain (red line), and cloud fractions from 10 KAZR dwells (thin colored lines) with their mean cloud fraction (black solid line) and standard deviation (dashed lines).

Figure 1b shows the horizontal distributions of the LES-simulated hydrometeor mixing ratio at 21:00 UTC on 9 June 2015 at 2.42 km and 4.19 km height above ground level. WRF successfully simulates the heterogeneity of a shallow cumulus field. We classify gridboxes with condensed hydrometeor mixing ratio greater than or equal to  $0.01 \text{ g kg}^{-1}$  as cloudy to define a cloud mask that is subsequently used for diagnosing the cloud fraction. Cloud-base heights are 1.8 km for the 2009 case and 2.4 km for the 2015 case, and cloud-top heights are 4.0 km for the 2009 case and 5.9 km for the 2015 case. Horizontal winds in the cumulus layers are predominantly from southeast for the 2009 case and northwest for the 2015 case. For the 2015 case in Figure 1b,

hydrometeor mixing ratios less than  $0.5 \text{ g kg}^{-1}$  dominate at the 2.42 km height, which is within the vicinity of cloud base. At 4.19 km, hydrometeor mixing ratios are higher than those at the cloud-base height, while the number of cloudy gridboxes is smaller. Similar hydrometeor mixing ratio distributions (e.g., liquid water content increasing with height) were simulated in the 2009 case that were validated by *Endo et al.* [2015] using aircraft observations. In addition, the distributions are also consistent with previous studies of cumulus clouds [e.g., *Warner, 1955; Grabowski and Clark, 1991*]. This study treats the LES-simulated clouds as a “truth” and explores the CF retrieval algorithm’s ability to obtain the LES-simulated clouds from the radar observables for typical or classic shallow convection cases.

## 2.2. CR-SIM

The CR-SIM is a scanning and profiling multiparametric radar simulator capable of emulating the interaction between transmitted polarized radar waves and rotationally symmetric hydrometeors. It inputs a simulated cloud field, and a forward model outputs conventional radar measurements such as reflectivity, Doppler velocity, and polarimetric variables. In addition to the radar forward model, CR-SIM simulates attenuated lidar backscatter at 905 nm and 532 nm, which correspond to the wavelengths of the Vaisala ceilometer and Micro Pulse Lidar, respectively. The radar frequency used in this study is 35.0 GHz (Ka band), with the radar operating in two configurations: zenith pointing to simulate KAZR observations and scanning to simulate the Ka-band SACR (Ka-SACR) observations. We include the effect of radar sensitivity when calculating the reflectivity. The sensitivity of each radar is governed by equation (1), where we set  $C = -50 \text{ dBZ}$  for both the KAZR and Ka-SACR. Assuming that the Ka-SACR location is the center of the LES domain, the  $Z_{\min}$  value is  $-27 \text{ dBZ}$  at a gridbox farthest from the radar between the cloud-base height and cloud-top height within the LES domain, and its value is nearly identical for both cases. In other words, cloudy grid points are guaranteed to be detected by KAZR and Ka-SACR if their reflectivity is greater than  $-27 \text{ dBZ}$ .

## 2.3. Implementing Cross-Wind Scanning and Pointing Strategies

Cross-Wind Range-Height Indicator (CWRHI) scanning is used for the Ka-SACR simulation [*Kollias et al., 2014a*]. During a CWRHI scan, the Ka-SACR samples the advected cloud field from  $0^\circ$  to  $180^\circ$  in elevation at a constant azimuth angle that is perpendicular to the mean wind direction in the cloud layer (Figures 1b and 1c). The sequence of 2-D CWRHI scans can be combined into 3-D cloud distributions by assuming that the distributions do not change significantly in time. The resolution of the 3-D cloud distribution data depends on radar sampling volume, the cloud translation speed, and radar scan speed. In this study, a CWRHI scan is performed every 30 s (equivalent to  $6^\circ \text{ s}^{-1}$  pedestal scan speed). For simplicity in sampling the cloud field using CWRHI scans, the cloud field is assumed to be stationary in time, other than cloud translation by the mean wind between scans, and the wind direction is assumed to be from the north with the actual wind direction disregarded. The mean cloud translation speed for each case is given by averaging the horizontal wind speed between the surface and the inversion level ( $4.2 \text{ m s}^{-1}$  for the 2009 case and  $6.0 \text{ m s}^{-1}$  for the 2015 case). For both cases, the instantaneous LES output is used from 21:00 UTC (16:00 central daylight time), which corresponds to the early afternoon when the clouds are largely driven by the surface heat fluxes and cloud top and base are roughly constant in time. The Ka-SACR is situated at the center of the domain ( $x = 0$ ).

The number of CWRHI scans ( $N$ ) to cover the LES domain (including clear or cloudy gridboxes) can be determined by the CWRHI scan speed ( $S$ ), the mean horizontal wind speed ( $V$ ), and the north-south distance ( $L$ ) of the LES domain,

$$N = \frac{SL}{180V}. \quad (2)$$

$N$  is 229 for the 2009 case and 143 for the 2015 case, where the difference is primarily attributable to the case mean wind speeds of, respectively,  $4.2 \text{ m s}^{-1}$  and  $6.0 \text{ m s}^{-1}$ .

The simulated radar reflectivity values and Ka-SACR CWRHI scan strategy are shown in Figures 1b and 1c, respectively. Near cloud-base height, the low mixing ratios result in low  $Z$  values of  $< -30 \text{ dBZ}$ . As a result, the Ka-SACR fails to detect most of these clouds farther from the radar in the center (Figure 1b). Near cloud top, the higher mixing ratios result in higher reflectivity ( $Z > -20 \text{ dBZ}$ ) and the range dependence of cloud detection is less pronounced. To guarantee detecting a certain reflectivity value, a sampling region is

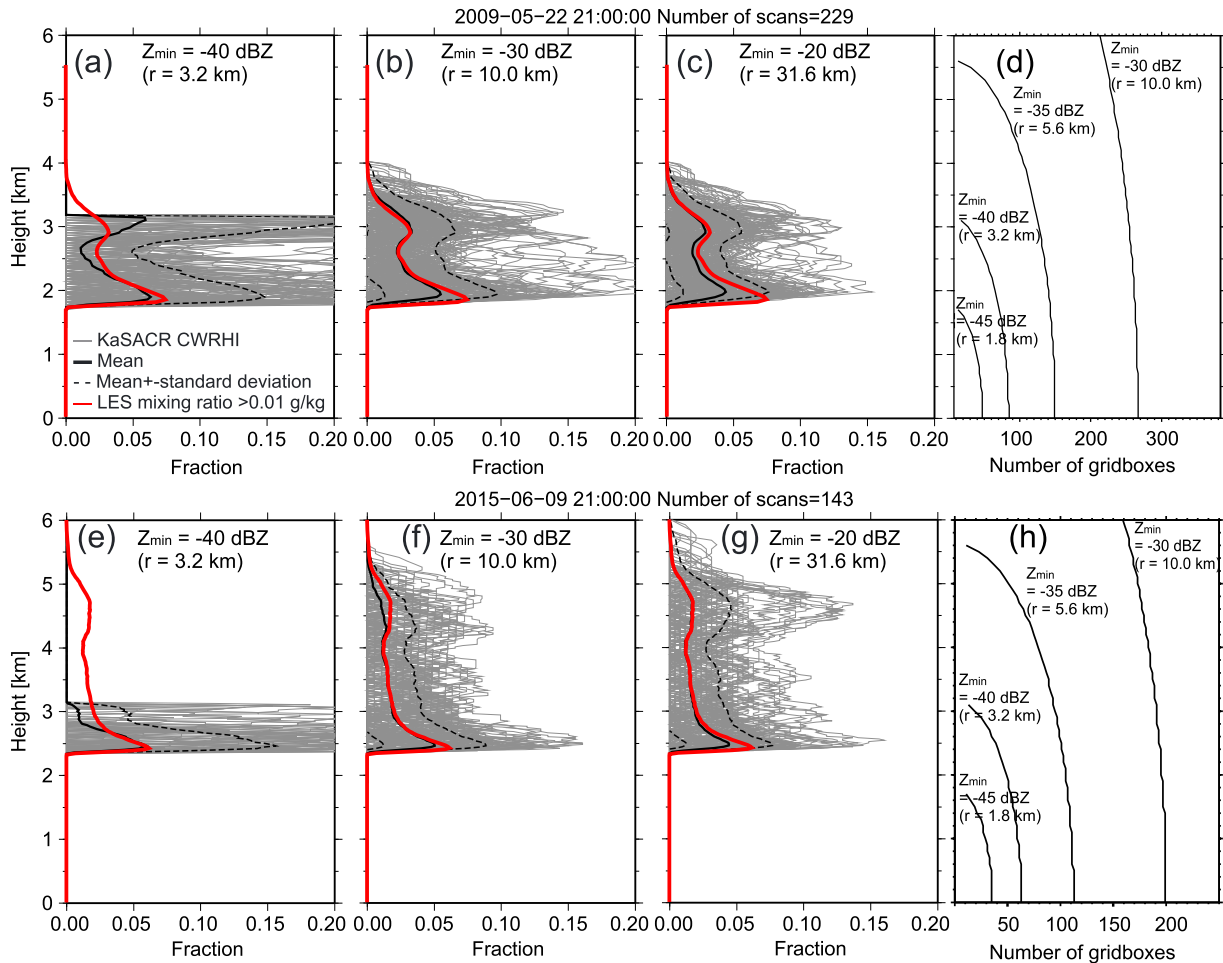


**Figure 2.** Cloud fraction profiles (CFPs) for different sampling regions determined by Ka-SACR  $Z_{min}$  of (a and e)  $-40$  dBZ, (b and f)  $-30$  dBZ, and (c and g)  $-20$  dBZ. (d and h) The numbers of LES gridboxes (clear or cloudy) occurring at a given height in the radial sampling regions for a CWRHI scan are denoted by their  $Z_{min}$ , ranging from  $-45$  dBZ to  $-30$  dBZ with  $5$  dB increments. Figures 2a–2d are for 22 May 2009, and Figures 2e–2h are for 9 June 2015. The number of gridboxes in the radial sampling region determined by  $Z_{min} = -20$  dBZ does not appear in Figures 2d–2h because the radial sampling region reaches the lateral boundaries of the LES domain and therefore includes the maximum number of gridboxes at a given height (384 for Figure 2d and 256 for Figure 2h). Note the different x axis ranges in Figures 2d and 2h. The red lines in Figures 2a–2c and Figures 2e–2g represent the domain-averaged CFPs from the LES with hydrometeor mixing ratios greater than or equal to  $0.01 \text{ g kg}^{-1}$ ; the gray lines represent CFP from each CWRHI scan, the solid black lines represent the mean CFP of CWRHI CFPs, and the dashed black lines represent the mean  $\pm 1$  standard deviation.

determined by a reflectivity sensitivity ( $Z_{min}$ ) isoline, as represented by blue lines in Figure 1c. Cloudy gridboxes with  $Z > Z_{min}(r)$  are collected within the sampling region. A sampling region defined by a low  $Z_{min}$  isoline can guarantee lower detectable  $Z$ , but the sampling region is smaller.

To assess the sampling of zenith profiling KAZRs, 10 KAZRs are simulated as being placed in the LES domain with equidistant spacing of  $2.56 \text{ km}$  along the east-west direction (Figure 1b). Figure 1d shows CFPs from the 10 KAZR dwells simulated by the CR-SIM. The LES domain-averaged CFP ( $CFP_{LES}$ ) is estimated by using only the model gridboxes with hydrometeor mixing ratios greater than or equal to  $0.01 \text{ g kg}^{-1}$ . It is clear that the individual KAZR CFPs exhibit great variability. The averaged CFP from the 10 KAZR's is in good agreement with  $CFP_{LES}$ ; however, it is unrealistic to expect 10 or more KAZRs at a ground-based site, particularly with the deployment taking into account hour-to-hour variability in wind direction.

### 3. Objective Determination of Cloud Fraction Profile

Figure 2 shows CFPs estimated from CWRHI scans along the east-west direction by using three different Ka-SACR sampling regions defined by the minimum sensitivity  $Z_{min}$  isolines of  $-40$ ,  $-30$ , and  $-20$  dBZ ( $CFP_{-40}$ ,  $CFP_{-30}$ , and  $CFP_{-20}$ ). These isoline sampling regions in a CWRHI scan are shown in Figures 2d

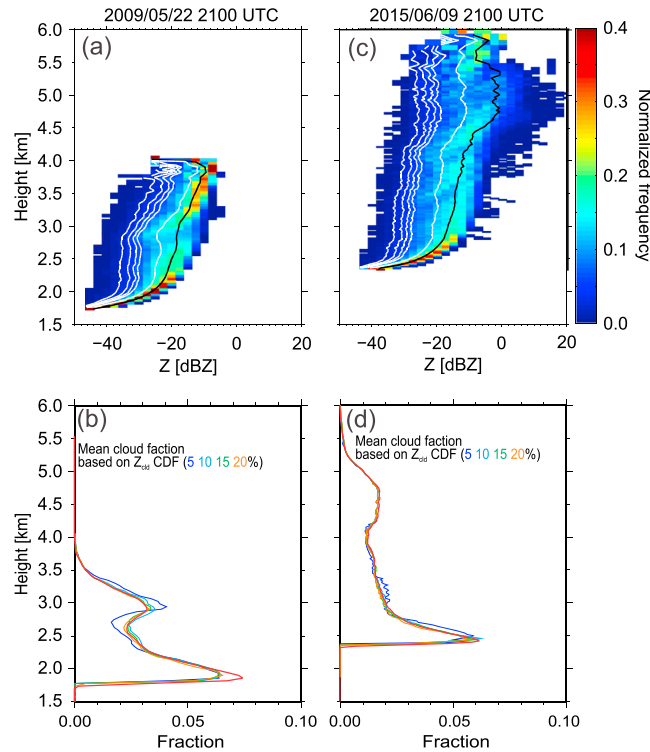


**Figure 3.** (a) Contoured frequency altitude diagram (CFAD) of  $Z$  with hydrometeor mixing ratios of  $>0.01 \text{ g kg}^{-1}$  for 22 May 2009. The black line represents the mean profile, and the white lines represent the cumulative probability density isolines of 5, 10, 15, 20, and 50% going from left to right. (b) Mean CFPs from CWRHI scans with sensitivities of 5% (blue), 10% (light blue), 15% (green), and 20% (orange), which correspond to the cumulative distribution function (CDF) isolines presented by white lines in Figure 3a, together with the LES domain-averaged CFPs (red). (c and d) Are as for Figures 3a and 3b, respectively, but for 9 June 2015.

$\text{CFP}_{-20}$  for both simulations is in good agreement with the  $\text{CFP}_{\text{LES}}$  at high levels, but it fails to capture the low-level cloud fraction for the same reasons as for  $\text{CFP}_{-30}$ . This analysis reveals the dilemma between sample (region) size and radar sensitivity. A large sampling region is desirable to reduce the uncertainty in the estimated CFP; however, the number of detectable cloudy gridboxes within the sampling region ultimately depends on the probability distribution function (PDF) of the cloud reflectivity  $Z_{\text{cld}}$  at each height, since the size of the sampling region limits the number of sampled cloudy gridboxes where  $Z_{\text{cld}} > Z_{\text{min}}(r)$ . This analysis also suggests that a combination of CFPs estimated for different  $Z_{\text{min}}$  could yield the best estimate for  $\text{CFP}_{\text{LES}}$ .

The contoured frequency by altitude diagrams (CFAD) [Yuter and Houze, 1995] of the Ka-SACR  $Z_{\text{cld}}$  for the two cases are shown in Figures 3a and 3c. For both cases, the PDF of  $Z_{\text{cld}}$  shifts toward higher values with altitude. This is consistent with clouds that contain little or no precipitation-size particles [Luke and Kollias, 2013] and implies that higher  $Z_{\text{min}}$  values, and thus a larger sampling region, can be used at higher altitudes. In addition to the CFAD, the cumulative distribution function (CDF) isolines at 5, 10, 15, 20, and 50% are displayed (Figures 3a and 3c). The CDF isolines are followed to determine the lowest sensitivity at which the isoline determines the sampling region as a function of height,  $Z_{\text{min}}(h)$ .  $Z_{\text{min}}(h)$  is used to change the desired size of the Ka-SACR sampling region with height to capture clouds with at least  $Z_{\text{cld}} > Z_{\text{min}}(h)$ . Figures 3b and 3d show the estimated CFPs based on the  $Z_{\text{min}}(h)$  sampling regions. The CFPs based on 5% CDF (blue lines) show the largest discrepancies for both cases, while those based on the 10, 15, and 20% CDF isolines exhibit convergence and close agreement with the  $\text{CFP}_{\text{LES}}$ . Convergence in the CFPs can be used as an indication of using the correct minimum CDF isoline for the determination of the CFP.

and 2h, noting that the  $-20 \text{ dBZ}$  isoline includes all gridboxes within the entire LES domain below cloud-top height. In these figures, radar sensitivity decreases with distance, as per equation (1), while the sampling region increases to include a greater number of gridboxes (see Figure 1c).

In both simulations, the mean  $\text{CFP}_{-40}$  captures well the  $\text{CFP}_{\text{LES}}$  near cloud base despite the small detection region/sample size (Figures 2d and 2h). At high levels (above 2.3 km), the mean  $\text{CFP}_{-40}$  overestimates the amount of cloud in the shallow case and underestimates it in the deeper case. The underestimation is due to the lack of radar sensitivity at that height, while the overestimation is likely the consequence of noise due to the small number of sampled gridboxes within the heterogeneous cloud field, where the limited sampling happens to sense more cloudy gridboxes relative to the cloud field mean. The larger number of gridboxes within the sampling region used in the estimation of the  $\text{CFP}_{-30}$  helps it approach the  $\text{CFP}_{\text{LES}}$  at high levels; however, the cloud amount at the low levels is underestimated due to the decreased hydrometeor mixing ratios despite the reduction in  $Z_{\text{min}}$ . Finally, the mean

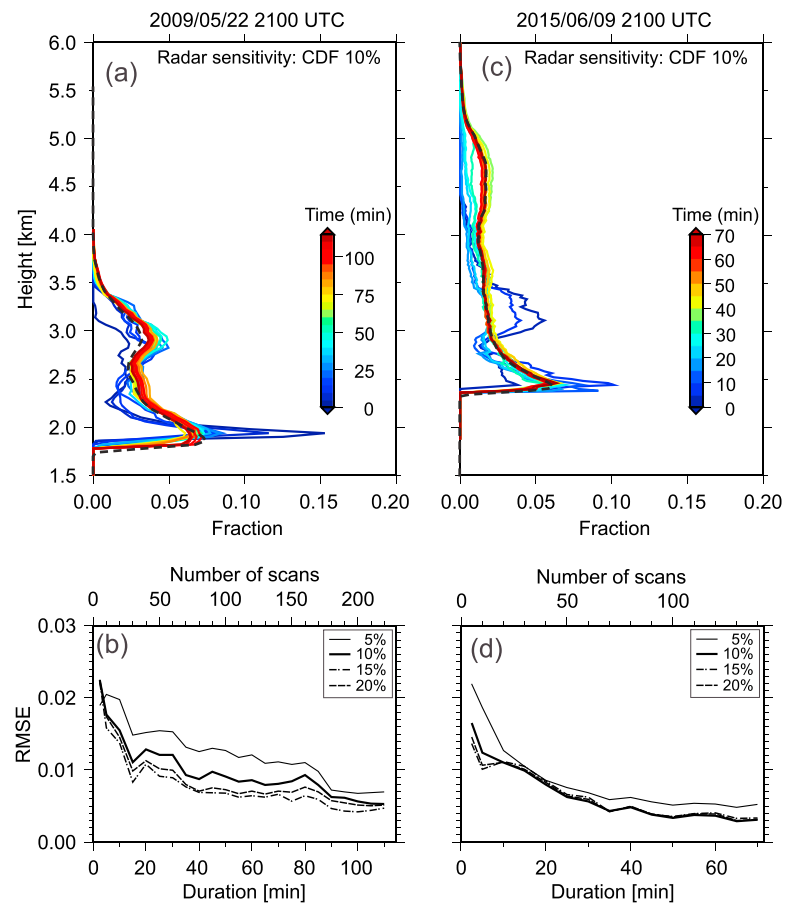


**Figure 4.** (a and c) Cloud fraction profiles corresponding to the 10% CDF isoline with changing scan duration time (hence, number of scans). (b and d) The root-mean-square error (RMSE) from the LES domain-averaged CFP for CDF isolines of 5% (thin solid line), 10% (thick solid line), 15% (dashed line), and 20% (dash-dotted line) as a function of duration time. Figures 4a and 4b are for 22 May 2009, and Figures 4c and 4d are for 9 June 2015. The black dashed line in Figures 4a and 4c represents the LES domain-averaged CFP for hydrometeor mixing ratio of  $\geq 0.01 \text{ g kg}^{-1}$ .

One remaining issue is the determination of the sampling time period (i.e., the number of CWRHI scans) needed to provide the best estimate of the CFP. Using the 10% CDF isoline, the CFPs are estimated for temporal intervals from 5 to 110 min for the 2009 case and 5 to 70 min for the 2015 case (Figures 4a and 4c). As expected, the CFPs converge to the  $\text{CFP}_{\text{LES}}$  as the sampling time increases. The root-mean-square error (RMSE) between the Ka-SACR CFP and the  $\text{CFP}_{\text{LES}}$  decreases as a function of sampling time is shown in Figures 4b and 4d. The RMSE values approach approximately 0.005 for the 2009 case and 0.003 for the 2015 case. The analysis suggests that a sampling time of approximately 35 min would be needed to reduce the RMSE values to less than 0.01 ( $<0.008$  for the 2009 case and  $<0.005$  for the 2015 case for the 10% CDF) and capture the domain-averaged CFP.

#### 4. Discussion and Conclusions

Evaluation of LES and cloud resolving models are some of the main drivers for developing and deploying scanning cloud radars. Zenith profiling radar and lidar observations traditionally have been used to estimate hourly-to-daily cloud fractions for several days to several months to study climatological cloud field properties [Hogan *et al.*, 2001; Kollias *et al.*, 2009]. Our analysis suggests that short-term (1–3 h) estimates of basic cloud field properties (e.g., CFP) of shallow convection from a single zenith profiling cloud radar are subject to large uncertainties. Impractical numbers of zenith profiling cloud radars (10 or more) within a small domain (30 km) are required to accurately estimate the CFP, even when assuming constant wind direction and stationary cloud fields. Scanning cloud radars have the advantage that they can sample a larger area; however,

the drop in radar sensitivity with range causes differing cloud detection limits with distance from the radar that must be considered carefully.

Two shallow cumulus cloud field distributions are provided by large eddy simulations using WRF with forcing conditions from the ARM SGP site. The model output is coupled with a radar simulator (CR-SIM) [Tatarevic and Kollias, 2015] to simulate the Ka-SACR observations from repeated CWRHI scans that sample the cloud field as it moves over the radar site. An analysis of the simulations demonstrates the Ka-SACR sample-sensitivity dilemma. Sampling a small region in the vicinity of the radar, wherein the radar sensitivity does not greatly decay, ensures higher sensitivity, but this results in an under sampling of the overall cloud field, and thus larger uncertainty in the CFP estimation. Alternatively, a larger sampling region ensures that more clouds are sampled, but the lower sensitivity farther from the radar underestimates the CFP due to undetected clouds. Using statistics of the CDF of cloud reflectivity  $Z_{\text{cld}}$  as a function of altitude, as depicted in a CFAD, an optimal  $Z_{\text{min}}(h)$  is determined by using a  $Z_{\text{cld}}$  CDF isoline that provides an optimum selection of region size and radar sensitivity. The  $Z_{\text{min}}(h)$  is subsequently used to determine the Ka-SACR sampling volume for the CFP estimation. The Ka-SACR observations need to be conducted for 35 min or more for the estimated CFP to converge with the LES-simulated CFP with an RMSE less than 1% for cloud fractions on the order of 5% (i.e., within 20% of the CFP). In our simulations,  $C = -50$  dBZ in equation (1) is used. A value of  $C = -69$  dBZ would be required to detect all clouds in the LES scene.

The conclusions of the presented study are limited to shallow convection where precipitation is not significant and large hydrometeor mixing ratio dominates at higher levels. Although this paper presented two shallow cumulus cases over the SGP, the proposed method for estimating CFP should be applicable to shallow convection in other environments. The presence of precipitation size particles would make the clouds more detectable at greater distances. However, if the precipitation rate is higher than  $1\text{--}2\text{ mm h}^{-1}$ , the effects of radar attenuation will come into play and need to be considered. Gaseous attenuation has not been considered in this study. For typical, summertime midlatitude conditions, the expected two-way gaseous attenuation at 35 GHz is about 2–3 dB [Kollias et al., 2014b, Figure 4c]. Gaseous attenuation is expected to shift the CFAD toward lower radar reflectivities by 2–3 dB and subsequently reduce the maximum sampling range. In the tropics, gaseous attenuation is higher (5–6 dB) and scanning millimeter wavelength radars have challenges operating at low-elevation angles. This analysis ignores other sources of errors such as the presence of insects and ground clutter. It also assumes that clouds move in the same direction and that the horizontal and vertical distributions of clouds do not change significantly over the analysis period. The latter assumption is particularly problematic since the naturally occurring diurnal cycle of clouds and temporal evolution of individual clouds cause them to change significantly over time periods on the order of an hour. Future work will need to optimize the balance of sampling time to achieve the necessary cloud sensitivity for changing cloud conditions, as the current work only examines the first issue by using a static cloud field. Even so, the presented work provides the first objective methodology of the estimation of a domain-averaged cloud field parameter from a scanning cloud radar.

#### Acknowledgments

Portions of this work are funded by the U.S. DOE Office of Science's Biological and Environmental Research Program through the Atmospheric Radiation Measurement Climate Research Facility. BNL components were also supported by the ASR and CMDV programs through contract DE-SC0012704. Battelle Memorial Institute operates PNNL under contract DEAC05-76RL01830. The LES data used in this paper are available by contacting the corresponding author (mariko.oue@stonybrook.edu). The source code and user manual for the Cloud Resolving Model Radar Simulator (CR-SIM) are available at <http://radarscience.weebly.com/radar-simulators.html>.

#### References

- Albrecht, B. A. (1981), Parameterization of trade-cumulus cloud amounts, *J. Atmos. Sci.*, *38*, 97–105, doi:10.1175/1520-0469(1981)038<0097:POTCCA>2.0.CO;2.
- Berg, L. K., and E. I. Kassianov (2008), Temporal variability of fair-weather cumulus statistics at the ACRF SGP site, *J. Clim.*, *21*, 3344–3358, doi:10.1175/2007JCLI2266.1.
- Berg, L. K., E. I. Kassianov, C. N. Long, and D. L. Mills Jr. (2011), Surface summertime radiative forcing by shallow cumuli at the Atmospheric Radiation Measurement Southern Great Plains site, *J. Geophys. Res.*, *116*, D01202, doi:10.1029/2010JD014593.
- Blyth, A. M. (1993), Entrainment in cumulus clouds, *J. Appl. Meteorol.*, *32*, 626–641, doi:10.1175/1520-0450(1993)032<0626:EICC>2.0.CO;2.
- Borquez, P., P. Kollias, and S. Giangrande (2014), First observations of tracking clouds using scanning ARM cloud radars, *J. Appl. Meteorol. Clim.*, *53*, 2732–2746, doi:10.1175/JAMC-D-13-0182.1.
- Browning, K. A., et al. (1993), The GEWEX Cloud System Study (GCSS), *Bull. Am. Meteorol. Soc.*, *74*, 387–399.
- Chandra, A. S., P. Kollias, and B. A. Albrecht (2013), Multiyear summertime observations of daytime fair-weather cumuli at the ARM Southern Great Plains Facility, *J. Clim.*, *26*, 10,031–10,050, doi:10.1175/JCLI-D-12-00223.1.
- de Rooze, S. R., and C. S. Bretherton (2003), Mass-flux budgets of shallow cumulus clouds, *J. Atmos. Sci.*, *60*, 137–151, doi:10.1175/1520-0469(2003)060<0137:MFBOSC>2.0.CO;2.
- Endo, S., A. M. Fridlind, W. Lin, A. M. Vogelmann, T. Toto, A. S. Ackerman, G. M. McFarquhar, R. C. Jackson, H. H. Jonsson, and Y. Liu (2015), RACORO continental boundary layer cloud investigations: 2. Large-eddy simulations of cumulus clouds and evaluation with in situ and ground-based observations, *J. Geophys. Res. Atmos.*, *120*, 5993–6014, doi:10.1002/2014JD022525.
- Ewald, F., C. Winkler, and T. Zinner (2015), Reconstruction of cloud geometry using a scanning cloud radar, *Atmos. Meas. Tech.*, *8*, 2491–2508, doi:10.5194/amt-8-2491-2015.

- Grabowski, W., and T. L. Clark (1991), Cloud-environment interface instability: Rising thermal calculations in two spatial dimensions, *J. Atmos. Sci.*, *48*, 527–546, doi:10.1175/1520-0469(1991)048<0527:CIIRC>2.0.CO;2.
- Gustafson Jr., W. I., and A. M. Vogelmann (2015), LES ARM Symbiotic Simulation and Observation (LASSO) implementation strategy, the U.S. Department of Energy, Office of Science, Office of Biological and Environmental Research. [Available at <https://www.arm.gov/publications/programdocs/doe-sc-arm-15-039.pdf>.]
- Gustafson, W. I., A. M. Vogelmann, X. Cheng, S. Endo, B. Krishna, Z. Li, T. Toto, and H. Xiao (2016), The LES ARM Symbiotic Simulation and Observation (LASSO) Alpha 1 Release, U. S. Department of Energy Atmospheric Radiation Measurement Climate Research Facility, doi:10.5439/1256454. [Available at <http://www.arm.gov/science/themes/lasso/releases> accessed 1-Aug-2016.]
- Hogan, R. J., C. Jakob, and A. J. Illingworth (2001), Comparison of ECMWF winter-season cloud fraction with radar-derived values, *J. Appl. Meteorol.*, *40*, 513–525, doi:10.1175/1520-0450(2001)040<0513:COEWSC>2.0.CO;2.
- Kollias, P., M. A. Miller, K. L. Johnson, M. P. Jensen, and D. T. Troyan (2009), Cloud, thermodynamic, and precipitation observations in West Africa during 2006, *J. Geophys. Res.*, *114*, D00E08, doi:10.1029/2008JD010641.
- Kollias, P., N. Bharadwaj, K. Widener, I. Jo, and K. Johnson (2014a), Scanning ARM cloud radars. Part I: Operational sampling strategies, *J. Atmos. Oceanic Technol.*, *31*, 569–581, doi:10.1175/JTECH-D-13-00044.1.
- Kollias, P., I. Jo, P. Borque, A. Tatarevic, K. Lamer, N. Bharadwaj, K. Widener, K. Johnson, and E. E. Clothiaux (2014b), Scanning ARM cloud radars. Part II: Data quality control and processing, *J. Atmos. Oceanic Technol.*, *31*, 583–597, doi:10.1175/JTECH-D-13-00045.1.
- Lamer, K., and P. Kollias (2015), Observations of fair-weather cumuli over land: Dynamical factors controlling cloud size and cover, *Geophys. Res. Lett.*, *42*, 8693–8701, doi:10.1002/2015GL064534.
- Lamer, K., A. Tatarevic, I. Jo, and P. Kollias (2013), Evaluation of gridded Scanning ARM Cloud Radar reflectivity observations and vertical Doppler velocity retrievals, *Atmos. Meas. Tech. Discuss.*, *6*, 9579–9621, doi:10.5194/amt-7-1089-2014.
- Larson, V. E., R. Wood, P. R. Field, J.-C. Golaz, T. H. Vonder Haar, and W. R. Cotton (2001), Small-scale and mesoscale variability of scalars in cloudy boundary layers: One-dimensional probability density functions, *J. Atmos. Sci.*, *58*, 1978–1994, doi:10.1175/1520-0469(2001)058<1978:SSAMVO>2.0.CO;2.
- Luke, E. P., and P. Kollias (2013), Separating cloud and drizzle radar moments during precipitation onset using Doppler spectra, *J. Atmos. Oceanic Technol.*, *30*, 1656–1671, doi:10.1175/JTECH-D-11-00195.1.
- Morrison, H., J. Curry, and V. Khvorostyanov (2005), A new double-moment microphysics parameterization for application in cloud and climate models. Part I: Description, *J. Atmos. Sci.*, *62*, 1665–1677, doi:10.1175/JAS3446.1.
- Myagkov, A., P. Seifert, M. Bauer-Pfundstein, and U. Wandinger (2016), Cloud radar with hybrid mode towards estimation of shape and orientation of ice crystals, *Atmos. Meas. Tech. Discuss.*, *8*, 9105–9163, doi:10.5194/amt-d-8-9105-2015.
- Neggers, R. A., A. P. Siebesma, and T. Heus (2012), Continuous single-column model evaluation at a permanent meteorological supersite, *Bull. Am. Meteorol. Soc.*, *93*, 1389–1400, doi:10.1175/BAMS-D-11-00162.1.
- Rémillard, J., P. Kollias, E. Luke, and R. Wood (2012), Marine boundary layer cloud observations in the Azores, *J. Clim.*, *25*, 7381–7398, doi:10.1175/JCLI-D-11-00610.1.
- Siebesma, A. P., and A. A. M. Holtslag (1996), Model impacts of entrainment and detrainment rates in shallow cumulus convection, *J. Atmos. Sci.*, *53*, 2354–2364, doi:10.1175/1520-0469(1996)053<2354:MIOEAD>2.0.CO;2.
- Siebesma, A. P., et al. (2003), A large eddy simulation intercomparison study of shallow cumulus convection, *J. Atmos. Sci.*, *60*, 1201–1219, doi:10.1175/1520-0469(2003)60<1201%3AALESIS>2.0.CO%3B2.
- Skamarock, W. C., et al. (2008), A description of the Advanced Research WRF version 3 NCAR Tech. Note NCAR/TN-475 + STR, 113 pp.
- Tatarevic, A., and Kollias, P. (2015), User's Guide CR-SIM SOFTWARE v 2.0, McGill University Clouds Research Group. [Available at <http://radarscience.weebly.com/radar-simulators.html>.]
- van Stratum, B. J. H., J. Vilá-Guerau de Arellano, C. C. van Heerwaarden, and H. G. Ouwersloot (2014), Subcloud-layer feedbacks driven by the mass flux of shallow cumulus convection over land, *J. Atmos. Sci.*, *71*, 881–895, doi:10.1175/JAS-D-13-0192.1.
- Vogelmann, A. M., et al. (2012), RACORO extended-term aircraft observations of boundary layer clouds, *Bull. Am. Meteorol. Soc.*, *93*, 861–878, doi:10.1175/BAMS-D-11-00189.1.
- Warner, J. (1955), The water content of cumuliform cloud, *Tellus*, *7*, 449–457, doi:10.1111/j.2153-3490.1955.tb01183.x.
- Wood, R., and P. R. Field (2011), The distribution of cloud horizontal sizes, *J. Clim.*, *24*, 4800–4816, doi:10.1175/2011JCLI4056.1.
- Xie, S. C., R. T. Cederwall, and M. H. Zhang (2004), Developing long-term single-column model/cloud system-resolving model forcing data using numerical weather prediction products constrained by surface and top of the atmosphere observations, *J. Geophys. Res.*, *109*, D01104, doi:10.1029/2003JD004045.
- Yuter, S. E., and R. A. Houze Jr. (1995), Three-dimensional kinematic and microphysical evolution of Florida cumulonimbus. Part II: Frequency distributions of vertical velocity, reflectivity, and differential reflectivity, *Mon. Weather Rev.*, *123*, 1941–1963, doi:10.1175/1520-0493(1995)123<1941:TDKAME>2.0.CO;2.
- Zhang, Y., and S. A. Klein (2013), Factors controlling the vertical extent of fair-weather shallow cumulus clouds over land: Investigation of diurnal-cycle observations collected at the ARM Southern Great Plains site, *J. Atmos. Sci.*, *70*, 1297–1315, doi:10.1175/JAS-D-12-0131.1.